PAPER

Check for updates

Investigation of photoelectric behaviors of silver sulfide particles in different surroundings†

Mengmeng Dong, Yanfei Lv, Xue Peng and Shichao Zhao [iD] *

Silver sulfide (Ag_2S) is a traditional semiconductor material, however, the photoelectric properties of Ag_2S particles under different environments are still lacking. In this paper, we reported the preparation of Ag_2S particles and their photoelectric properties under different environments. Results showed that the photoelectric performance of Ag_2S particles was closely related to the environment. It was found that a copper phthalocyanine coating could improve the light response, the mixture of alcohols and air could increase the photoconductivity, and the mixture of carbon disulfide and air could decrease the photoconductivity. The mechanism of the effect of various experimental conditions on photoelectric properties was also discussed.

1. Introduction

Silver sulfide (Ag_2S) is an important inorganic semiconductor material with properties of both metal and insulator.[1] Silver sulfide has a wide range of potential applications in sensors, nitrogen and antibiotics removal, antibacterial agents, hydrogen production, photocatalysts, solar cells, fiber lasers, near-infrared fluorescence biological imaging, photonics, random network reservoir computing devices *etc.*[2–17] Apart from the above applications, in recent years, more and more attention has been focused on its potential application in photodetectors due to their near-infrared transparency, low cost, non-toxicity and compatibility with silicon integrated circuits.[18–20] Kang *et al.* prepared a photodetector by assembling Ag_2S nanoparticles on the silicon oxide substrate and covering a layer of graphene on the top of Ag_2S nanoparticles. They found that the photodetector showed a high photoresponse of 2723.2 A W^{-1} under 550 nm illumination with 0.89 mW cm^{-2}.[21] Chen *et al.* prepared a Ag_2S/ZnO hybrid photodetector. They found that their photodetector is highly sensitive to wavelengths from 400 nm to 1100 nm and the response is fast, less than 5 ms.[22] Ismail *et al.* and Tretyakov *et al.* prepared Ag_2S/Si hetero-junction photodetectors.[20,23] Ismail *et al.* found that the properties of the detector were dependent upon the Ag_2S nanotube deposition time and the maximum responsivity was found to be *ca.* 0.5 A W^{-1} at 850 nm.[23] Tretyakov *et al.* reported the photovoltaic effect of the detector based on Ag_2S quantum dots and Si heterostructure and discussed the mechanisms of infrared absorption: crystal defect absorption of Ag_2S or surface state

absorption of Si.[20] Tang *et al.* prepared $Ag_2Se@Ag_2S$ core–shell nanocrystals by an improved solution reaction method, and found that the nanocrystals showed sensitive near-infrared photodetection.[24] Lei *et al.* reported flexible self-powered Ag_2S photodetector by sandwiching silver film between Ag_2S and organic substrate for the first time, and results showed that the device could withstand *ca.* 4000 bending cycles without performance decay.[25]

It is well known that it is difficult to obtain single crystal of Ag_2S. Therefore, the Ag_2S used in the above devices generally presents in the form of polycrystalline or dispersed particles. The discontinuity or poor crystal quality, however, can greatly reduce the photoelectric performance and hinder the practical application. We previously reported that poly-(N,N'-bis-4-butyl-phenyl-N,N'-bisphenyl)benzidine and phenyl-C61-butyric acid methyl ester on the isolated tungsten disulfide (WS_2) mono-layers could improve the photoelectric properties of WS_2.[26] The organic carrier transport layer plays an important role in the formation of conduction channel and in the improvement of the exciton separation.[26] Photoelectric performance tests have been usually carried out in atmospheric environment. The effects of carbonaceous and sulfurous gases on photoelectric properties are usually ignored. Herein, we developed a simple method to deposit a continuous copper phthalocyanine (CuPc) film on the surface of Ag_2S particle film, and photoelectric performances were examined in air mixed with methanol, ethanol, propyl alcohol, butyl alcohol and carbon disulfide (CS_2), respectively. We found Ag_2S showed completely different photoelectrical properties in carbon disulfide, which can be used for selective detection of the toxic gas of CS_2. It is well known that the selectivity of gas sensors based on semiconductor particles is difficult to achieve. Our results may provide a way to detect gas by using photoelectric performance.

College of Materials & Environmental Engineering, Hangzhou Dianzi University, Hangzhou, 310018, P. R. China. E-mail: lvyanfei@hdu.edu.cn; zhaoshichao@hdu.edu.cn

2. Experimental

2.1 Chemicals

Silver and sulfur were used as the precursor of Ag_2S. Silver (99.95%), sulfur powders (99.99%), methanol (CH_3OH, AR), ethanol (CH_3CH_2OH, AR), n-propyl alcohol ($CH_3CH_2CH_2OH$, AR), n-butyl alcohol ($CH_3CH_2CH_2CH_2OH$, AR) and carbon disulfide (CS_2, AR) were purchased from Aladdin (Shanghai, China).

2.2 Preparation of Ag_2S particles film

Silver sulfide particles film was grown on the glass substrate by the reaction between silver and sulfur. Silver film with a thickness of 300 nm was firstly deposited on the glass substrate by conventional thermal evaporation under 5×10^{-4} Pa with a deposition rate of 12 nm min^{-1}. Then sulfur powders were loaded in a quartz boat. The silver film was covered on the quartz boat. After that, the quartz boat was put into a quartz tube. The quartz tube was vacuumed with argon (20 sccm) as a protective gas for 15 minutes to remove the air. Then the quartz tube was sealed at ca. one atmosphere and heated to 250 °C from room temperate with a rate of 10 °C min^{-1}. After heating at 250 °C for 30 minutes, the quartz tube was cooled down to room temperature naturally and the Ag_2S was obtained.

2.3 Preparation of Ag_2S photodetector with CuPc film

The photodetector was prepared by the deposition of CuPc film and silver electrode layer on the Ag_2S particles grown on the glass substrate in turn. The CuPc layer was deposited by vacuum thermal evaporation process.[27] The deposition pressure was set at less than 6×10^{-4} Pa. The thickness of the CuPc is ca. 7 nm. The silver electrode was vaporized onto the CuPc film using a mask. The channel width of the detector is 30 μm, and the length is 100 μm. The schematic diagram of the photodetector is shown in Fig. 1a.

2.4 Preparation of photodetector based on Ag_2S particles

Aurum (Au) interdigital electrode was patterned onto the alumina ceramic substrate using photolithography by evaporation. Then Ag_2S particles grown on the glass substrate (see 2.2) were scraped and sonicated in deionized water. Ag_2S particles dispersed in water were dropped onto the surface of

Aurum interdigital electrode and dried in air to form the detector, as shown in Fig. 1b.

2.5 Characterization

X-ray diffraction (XRD) was carried out on a Thermo ARLXTRA. Field emission scanning electron microscopy (FESEM) coupled with energy dispersive X-ray spectroscopy (EDS) were conducted on a FEI Apreo S HiVac. Raman spectroscopy was performed on an HR Evo Nano with a 532 nm laser. Ultraviolet visible near infrared (UV-VIS-NIR) absorption was conducted by using a Shimadzu UV-3600. Electrical measurements of the Ag_2S coated with CuPc film were conducted on an Agilent 4200SCS and a LakeShore TTPX. Photoelectric characteristics were examined under the irradiation of a 500 nm laser with a power of 2.5 mW cm^{-2}. Photoconductive tests of the photodetector based on Ag_2S particles under different atmospheres (methanol, ethanol, n-propyl alcohol, n-butyl alcohol and CS_2) were conducted on a Keysight 34461A with a commercial light-emitting diode with a central wavelength of ca. 470 nm. The power of the diode was set at ca. 2.0 mW cm^{-2}. A typical response test cycle was about 80 s. In this experiment, the detector was put in a home-made plastic chamber (100 ml) connected to air. Chemical (25 μl) was injected into the chamber. After injection, the chamber was sealed. As the liquid reagents evaporated, the concentration of the gas of alcohols and CS_2 in the air increased from zero to saturation. The chamber was thoroughly cleaned using deionized water and gas flushing before experiment.

3. Results and discussion

3.1 XRD of Ag_2S

Fig. 2 shows the XRD patterns of Ag_2S particles grown on the glass substrate. The peaks at 31.5°, 33.6°, 34.4°, 34.7°, 36.8°, 37.7°, 40.8° are attributed to the diffraction peaks of monoclinic crystals of Ag_2S (JCPDS, 14-0072), corresponding to the (−112), (120), (−121), (022), (013), (−103) and (031) planes, respectively. No diffraction peaks except Ag_2S were found, indicating that the product was mainly silver sulfide. The average width of the three
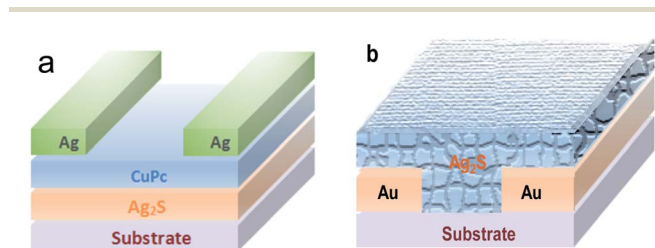

Fig. 1 The illustration of two different photodetectors: (a) based on the Ag_2S/CuPc hybrid film; (b) Ag_2S particles deposited on Au interdigital electrode.
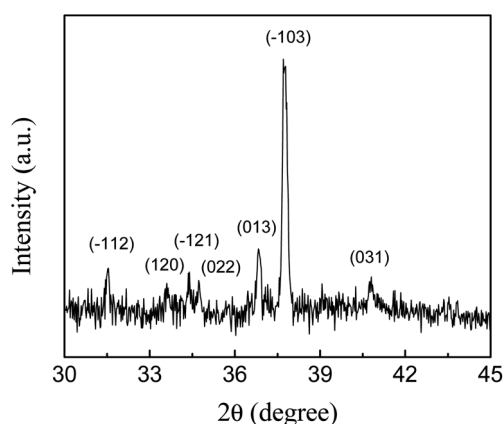

Fig. 2 X-ray diffraction patterns of Ag_2S particles on glass substrate prepared by the reaction of silver and sulfur vapor at 250 °C.

relatively strong peaks of (013), (−103) and (031) is $0.16° \pm 0.03°$, according to Scherrer formula and take into account of the instrument error, the average size of Ag_2S particles is estimated to be larger than 48 nm.[28] The intensity of the diffraction of the Ag_2S is low. The signal intensity of the strongest diffraction peak (−103) is only *ca.* ten times that of the noise signal. We believe that the silver film vaporized and sublimated away during the Ag_2S growth at relatively high temperature, resulting in the poor crystallinity. XRD patterns of samples grown at low temperature are shown in Fig. S1.† The strongest peak of different samples appears at different positions, indicating that the synthesizing condition has an effect on the crystallization quality. In the sample grown at 100 °C, sulfur impurity was found (Fig. S1a†). Therefore, low temperature is not beneficial for the pure Ag_2S growth. It is difficult to obtain high-quality Ag_2S by chemical reaction between the metal silver film and sulfur vapor.

3.2 Raman

Fig. 3 shows the Raman spectra of Ag_2S particles for different laser irradiation time. It can be seen that broad peaks exist in the low-frequency region, centered at *ca.* 53, *ca.* 198 and *ca.* 460 cm^{-1}. The peak at *ca.* 53 cm^{-1} is corresponding to A_g mode of Ag_2S.[29] The peaks at *ca.* 198 and *ca.* 460 cm^{-1} are due to the first- and second-order longitudinal optical phonon modes in monoclinic α-Ag_2S.[30] The existence of these broad peaks can be attributed to the lattice disorder and/or silver vacancies formed during the crystal growth or laser illumination during the Raman test.[31] In addition, a shoulder at *ca.* 273 cm^{-1} is attributed to the radial vibrations of $(AgS)_n$ clusters.[30] In the high-frequency region, there exist two peaks at *ca.* 1230 and *ca.* 1422 cm^{-1}, respectively. These peaks were also observed by other research groups when the Raman test was carried out with high power laser irradiation. Martina *et al.* assumed that these peaks were due to the photo-decomposition products.[32] We observed that the intensity of the Raman peaks decreased with

the extension of Raman test time, indicating that the photo-decomposition of Ag_2S occurred during laser irradiation. These peaks *ca.* 1230 and *ca.* 1422 cm^{-1}, are related to the photo-decomposition products of Ag_2S, such as silver and sulfur oxides.[29,30] We assumed that Ag_2S would react further with oxygen in air to form silver oxide (Ag_2O). The existence of Ag_2O is evidenced by the appearance of two peaks at 551 and 1074 cm^{-1} in Fig. 3f, which are corresponding to the Ag–O stretching/bending modes.[33]

3.3 FESEM and EDS

FESEM was conducted to characterize the morphology of Ag_2S particles.[34] It was observed that Ag_2S particles were dispersed on the substrate, and in some areas the particles sticked together (Fig. 4a). The silver sulfide particles exhibit a pyramid shape, indicating that Ag_2S is crystallized. The size distribution of Ag_2S domains is not uniform, ranging from *ca.* 55 nm to *ca.* 470 nm, with most domains at *ca.* 150 nm. The results are consistent with the previous XRD results. The composition of the particles was analyzed by EDS.[35] Fig. 4b–d is the overlay of sulfur (S) and silver (Ag) EDS maps, S EDS map, and Ag EDS map, respectively. The coincidence of these three maps proves that the particles are Ag_2S. The ratio of Ag : S is *ca.* 62.67 : 37.33 according to the EDS data, indicating the presence of silver vacancies in the Ag_2S crystals.

3.4 UV-VIS-NIR absorption

Fig. 5 shows the UV-VIS-NIR absorption spectrum of Ag_2S particles. An absorption edge in the near-IR region (0.65–1.5 eV) is due to Ag_2S particles. Tauc plot was used to estimate the bandgap energy as shown in the insert in Fig. 5.[36] Herein, the plot was generated by plotting $(Ah\nu)^2$ as a function of photon energy $h\nu$, where A represents the absorption value. The
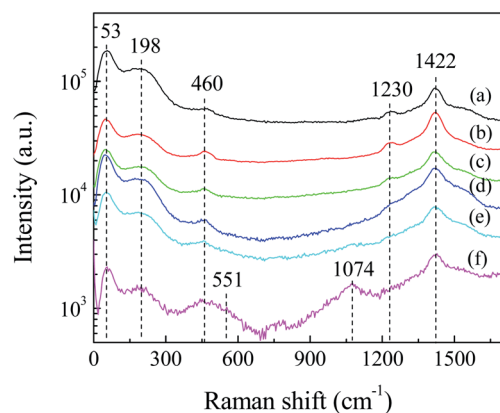

Fig. 3 The time evolution of Raman spectra of Ag_2S particles: (a) 30 s, (b) 210 s, (c) 390 s, (d) 570 s, and (e) 750 s, and (f) 930 s, respectively. The Raman spectrum was integrated for 30 s, with continuous laser illumination. The signal of curve (a) was amplified by five times. Apart from (a), the data were measured at same location.
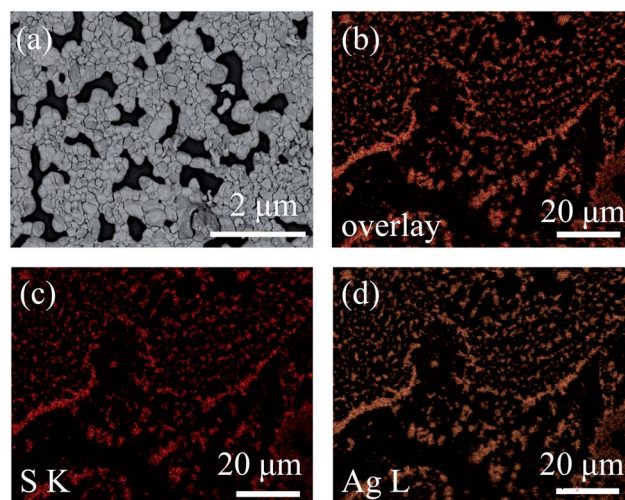

Fig. 4 Typical FESEM image and EDS mappings of Ag_2S particles on glass substrate prepared by the reaction of silver and sulfur vapor at 250 °C: (a) FESEM image, (b) overlay of S and Ag EDS maps, (c) S EDS map, and (d) Ag EDS map. The scale bar in (a) represent 2 µm, and 20 µm in (b)–(d).
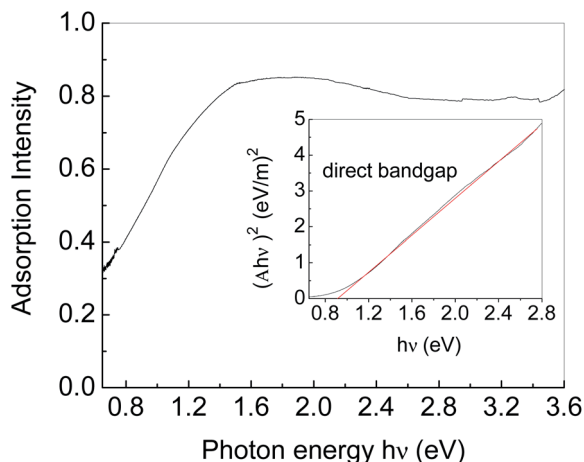
Fig. 5 UV-VIS-NIR absorption spectrum of Ag$_2$S particles grown on glass substrate through the reaction of silver and sulfur vapor at 250 °C. The insert shows the Tauc plot, where A represents the absorption value of Ag$_2$S particles.

Fig. 6 I–V curves of Ag$_2$S/CuPc hybrid film with (a) and without (b) laser illumination.

horizontal axis of the insert figure corresponds to the photon energy $h\nu$ and the vertical axis corresponds to the value of $(Ah\nu)^2$. The plot behaves as a linear function near the absorption edge, indicating that Ag$_2$S is a direct band gap semiconductor. The intercept of the extension of the linear part on the horizontal axis is considered as the bandgap energy. The bandgap energy of Ag$_2$S particles is calculated to be *ca.* 0.92 eV, consistent with those previously reported.[37–39] In addition to the absorption edge, there is an Urbach tail on the low energy side.[40] The Urbach tail is generally associated with low crystallinity, defects, and inter-grain depletion.[28,41] We fitted the Urbach tail by an exponential function, and found the Urbach energy was *ca.* 200 meV, indicating the low crystallinity of the Ag$_2$S particles we obtained.[41]

3.5 Photoelectric properties of Ag$_2$S with CuPc coating

Fig. S2† show the current–voltage (I–V) curve of Ag$_2$S film under irradiation at 500 nm. It was found that the dark and light currents overlapped with the open circuit test current. The result demonstrated the pure Ag$_2$S film was nonconductive. As can be seen from the FESEM image (Fig. 4), the continuity of the film is poor, thereby rendering the film nonconductive. After being coated with CuPc, the photocurrent was evaluated. Fig. 6 shows the I–V curves of the device based on Ag$_2$S/CuPc hybrid film with or without light. The light current is larger than the dark current. Fig. 7 shows the current–time curve of the device. The device shows a stable photoelectric performance in a limited number of test cycles. The photocurrent and on/off ratio increase with the increase of time (Fig. 7a), which is related to the gas desorption. The rise/decay time (in Fig. 7b) is *ca.* 160 ms, which is faster than that of pure CuPc.[27] Kim *et al.* investigated the photodetector based on Ag$_2$S and carbon nanotubes.[42] The rise/decay time they obtained is one/two orders of magnitude slower than that of our results. Therefore, we assumed the presence of CuPc could improve the photo-electric properties of Ag$_2$S. The conduction type of Ag$_2$S
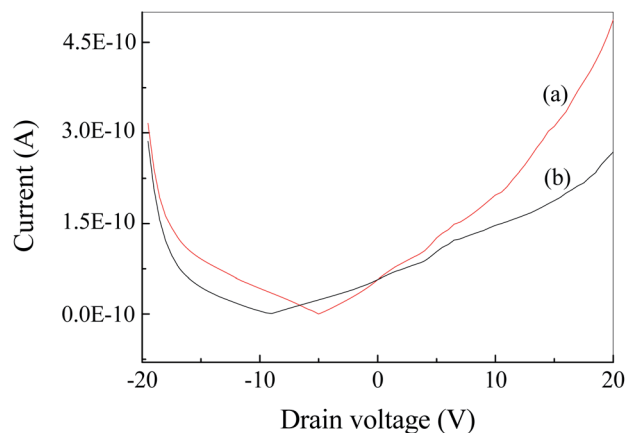
was proved to be n-type by hot-probe method (Fig. S3†).[43] After the formation of heterogeneous structure of n-type Ag$_2$S and p-type CuPc, a built-in electric field is formed between them, promoting the separation of photogenerated electron–hole pairs.[27] The separated electrons and holes are transferred to CuPc, which acts as a carrier transport channel, thereby enhancing the photoelectric performance of the device.

3.6 Photoelectric properties of Ag$_2$S particles in different atmospheres

In order to study the effects of atmosphere on the photoelectric properties, the photoconductance test of photodetector based on Ag$_2$S particles were carried out in air containing alcohol homologue and CS$_2$. Fig. 8a shows the time dependent resistance of Ag$_2$S particles with/without light irradiation in air and CH$_3$OH. It was observed that the resistance decreased during the light exposure and recovered after the light was turned off. This cycle was repeatable within the time frame of the test. The resistance decreases by *ca.* 0.9% after illumination. The main reason for the decrease of the resistance as the light turns on is due to the generation of photocurrent. The shape of the peak in Fig. 8a is different from that in Fig. 6b, where the former is blade and the latter is rectangular. Same phenomenon can be found in Fig. 8b–d. The resistance of the photo detector in an inert atmosphere is great and out of the range of Keysight 34461A, shown in Fig. S4.† The photocurrent effect was not observed. It is believed that the difference of the peak shape in Fig. 7 and 8 is related to adsorption–desorption kinetics of gas molecules on Ag$_2$S surface. The blade shape indicates a longer time to reach adsorption equilibrium. Different from the photoelectric properties of Ag$_2$S coated with CuPc, the resistance of Ag$_2$S particles surrounded with alcohol atmosphere cannot reach a steady state even after a long time. For example, the resistance of *n*-butyl alcohol adsorbed Ag$_2$S particles was found to be kept increasing even after the illumination stopped for 3 minutes. Therefore, it is not appropriate to use up/decay time to characterize the response time. Herein, exponential functions were used to fit the data in Fig. 8 and the calculated
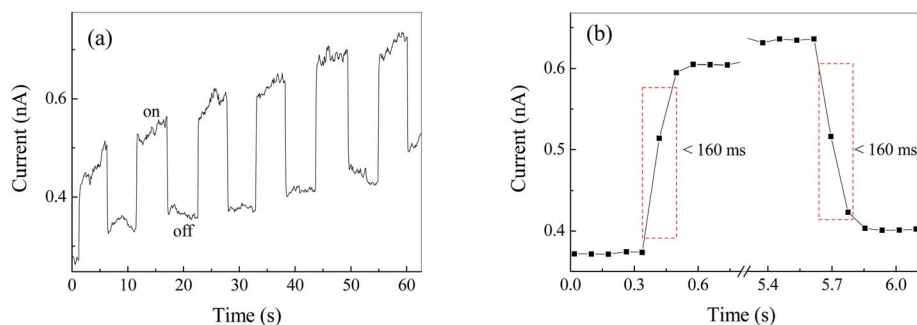
Fig. 7 Current–time curve of Ag$_2$S/CuPc hybrid film with/without laser illumination: (a) the current–time curve with laser on/off; (b) magnified image of (a) in the range from 63.3 to 69.3 s, decent showing the rise and decay time of the photodetector. The drain voltage of the photodetector is 20 V. The internal of data collection is 80 ms.

exponential constant was used to characterize the response time.

The part of the curve where the resistance drops after illumination is fitted by exponential decay function. The exponential decay constants are *ca.* 34 ± 11 s^{-1}, 582 ± 318 s^{-1}, 41 ± 7 s^{-1} and 57 ± 20 s^{-1} corresponding to the detector exposed to methanol, ethanol, *n*-propyl alcohol and *n*-butyl alcohol, respectively. Except ethanol, the decay time increases with the increase of carbon atoms in alcohol homologue, indicating that the resistance of the detector is related to the size of adsorbed gas molecule.

It was observed that the background of resistance–time curves decreased with the increase of time. As the alcohol gases, reductive molecules, adsorb on the surface of n-type Ag$_2$S particles, the energy band near the grain boundaries bends down, resulting in the decrease of the resistance. Therefore, with the extension of time, the adsorption molecules increase and the resistance decreases. Adsorption of gas molecules leads to the longer response time.

Fig. 9 shows the illumination dependent resistance–time curve of Ag$_2$S photodetector exposed to CS$_2$ and air. Contrary to the previous data in Fig. 8, the resistance increased sharply to a maximum by *ca.* 5.4% and decreased slowly during the
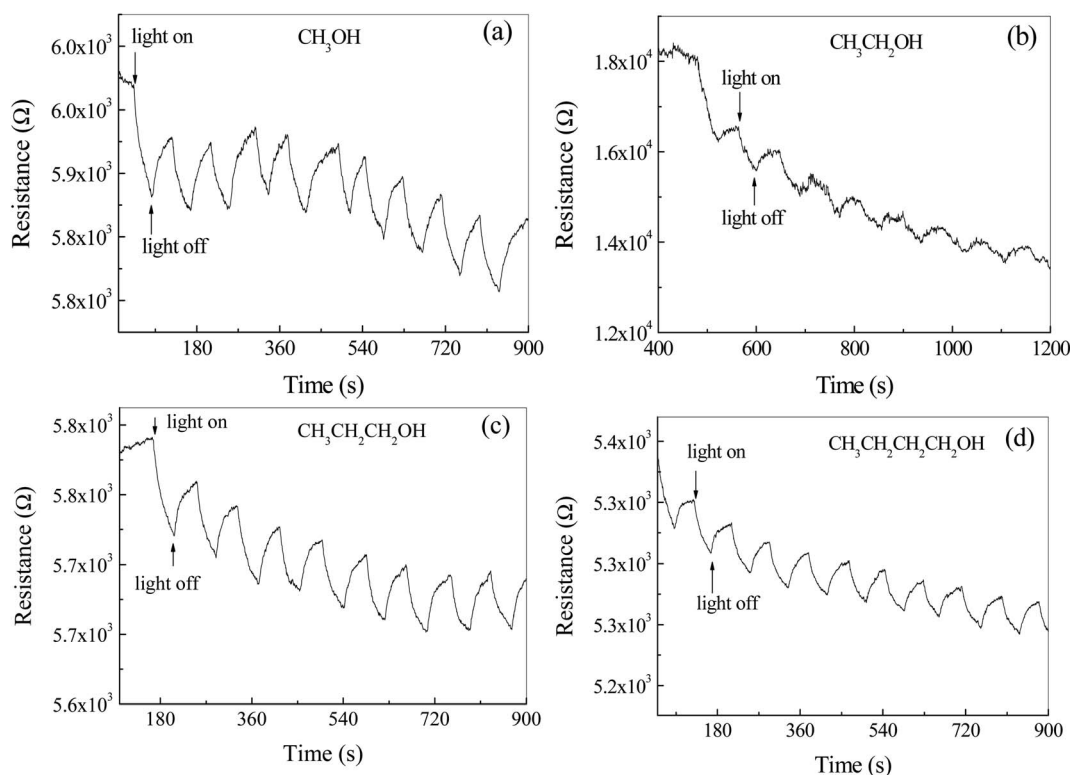

Fig. 8 The resistance–time curves of Ag$_2$S particles with/without light exposure in air mixed with (a) methanol (CH$_3$OH), (b) ethanol (CH$_3$CH$_2$OH), (c) *n*-propyl alcohol (CH$_3$CH$_2$CH$_2$OH), and (d) *n*-butyl alcohol (CH$_3$CH$_2$CH$_2$CH$_2$OH), respectively.
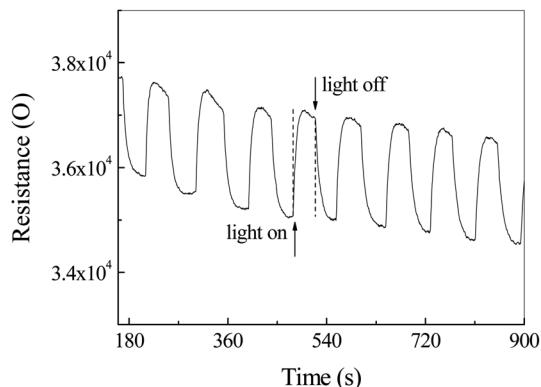
Fig. 9 The resistance–time curve of Ag$_2$S particles in a mixture of air and carbon disulfide (CS$_2$) with/without light irradiation.

illumination. As the light turned off, the resistance reduced dramatically to a minimum. This phenomenon can be mainly attributed to the selective adsorption of CS$_2$ and the resulting energy band bending of Ag$_2$S, rather than a photoconductivity effect.

It is well known that, in colloidal chemistry, substances preferentially adsorb ions of the same ions as those contained in the substance itself. Herein, we suppose a dense layer of CS$_2$ is adsorbed on the surface of the Ag$_2$S particles by selective chemisorptions and oxygen molecules are pushed away from the particle surface. The CS$_2$ releases an electron to Ag$_2$S to form CS$_2^+$ cations adsorbed on the Ag$_2$S surface, resulting in the formation of an electron accumulation layer at the surface of Ag$_2$S and the downward energy band bending of Ag$_2$S (Fig. 10a). As a result, the resistance drops to a minimum. CS$_2$ desorption and oxygen adsorption occurred under illumination. We assumed that the photoinduced oxidation promotes the CS$_2$ desorption. Oxygen molecules acquire electrons and exist on the surface of Ag$_2$S in the form of negative ions, forming a depletion layer at the boundary, resulting in an upward

bending of the energy band and an increase in resistance (Fig. 10b).[44] Indeed, the specific mechanism of adsorption and desorption is still unclear, and further research is needed.

4. Conclusion

In this study, Ag$_2$S photodetectors were prepared and its photoelectric properties were examined in the presence of CuPc coating, air, alcohol gases and carbon disulfide. Results show that the detector based on Ag$_2$S particles covered with CuPc film exhibits faster response time, and that the CuPc coating can improve the photoelectric performance by forming a built-in field. Our results showed organic and inorganic semiconductor hybrid is a convenient way to prepare photodetectors with low cost and high performance. In addition, it was found that the photoelectric performance of the device is sensitive to the atmospheres. The response time of the device based on pure Ag$_2$S particles is reduced due to the adsorption of alcohol gases. Different from alcohol gas, the presence of carbon disulfide increases the resistance of the detector, which can be used for the selective detection of CS$_2$. In addition, our results provide a possible way to study gas adsorption behavior by photodetector.

Author contributions

Yanfei Lv conceived and designed the experiments; Mengmeng Dong and Xue Peng performed the experiments; Shichao Zhao performed the data analyses and wrote the paper.

Conflicts of interest

The authors declare no conflict of interest.

Acknowledgements

References

1 N. S. S. R. Barman, A. K. Shukla and D. D. Sarma, *Phys. Rev. B: Condens. Matter Mater. Phys.*, 1996, **53**, 3746.
2 Q. Wang, H. S. Yin, Y. L. Zhou, J. Wang and S. Y. Ai, *J. Hazard. Mater.*, 2021, **414**, 125293.
3 W. C. Geng, D. L. Li, J. L. Sang, L. L. Pan, Z. L. Jiang, C. Liu and Y. J. Li, *J. Mater. Chem. B*, 2020, **8**, 10346–10352.
4 J. H. Feng, Y. Y. Li, Z. Q. Gao, H. Lv, X. B. Zhang, Y. H. Dong, P. Wang, D. W. Fan and Q. Wei, *Sens. Actuators, B*, 2018, **270**, 104–111.
5 A. R. Jang, J. E. Lim, S. Jang, M. H. Kang, G. Lee, H. Chang, E. Kim, J. K. Park and J. O. Lee, *Appl. Surf. Sci.*, 2021, **562**, 150201.
6 C. Cao, J. Huang, C. N. Yan, X. X. Zhang and Y. X. Ma, *Sci. Total Environ.*, 2021, **777**, 145171.
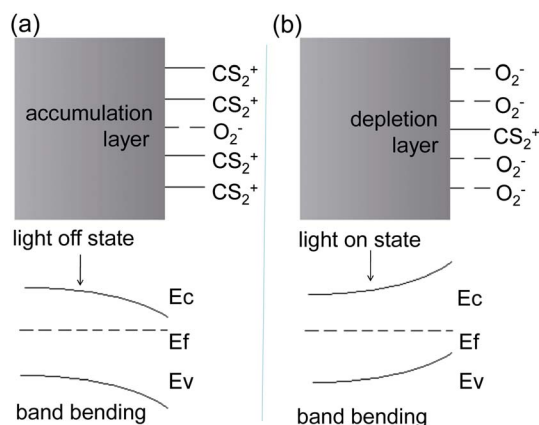7 H. A. Alshamsi, F. Beshkar, O. Amiri and M. Salavati-Niasari, *Chemosphere*, 2021, **274**, 129765.

Fig. 10 Schematic illustration of gas adsorption over Ag$_2$S particles and corresponding band bending: (a) CS$_2$ adsorption and downward bending; (b) oxygen (O$_2$) adsorption and upward bending under light irradiation. *Ec*, *Ef* and *Ev* represent conduction band, Fermi level and valence band, respectively.

8 X. Gao, H. X. Li, X. H. Niu, D. Y. Zhang, Y. Wang, H. Y. Fan and K. J. Wang, *J. Inorg. Biochem.*, 2021, **220**, 111456.

9 B. W. He, C. B. Bie, X. G. Fei, B. Cheng, J. G. Yu, W. Ho, A. A. Al-Ghamdi and S. Wageh, *Appl. Catal., B*, 2021, **288**, 119994.

10 X. B. Dong, S. J. Wang, Q. Wu, K. Y. Liu, F. O. Kong and J. X. Liu, *J. Alloys Compd.*, 2021, **875**, 160032.

11 C. J. Chang, M. C. Teng, J. Chen, Y. G. Lin and C. Y. Chen, *Appl. Surf. Sci.*, 2021, **558**, 149875.

12 I. Hwang, M. Seol, H. Kim and K. Yong, *Appl. Phys. Lett.*, 2013, **103**(2), 023902.

13 W. F. Luo, Y. J. Ren, J. J. Feng, X. H. Li, S. Y. Lv, M. J. Qu, L. R. Jing and X. H. Chen, *Nanotechnology*, 2021, **32**, 355202.

14 C. P. Ding, Y. J. Huang, Z. Y. Shen and X. Y. Chen, *Adv. Mater.*, 2021, **33**(32), 2007768.

15 H. Hadiyawarman, Y. Usami, T. Kotooka, S. Azhari, M. Eguchi and H. Tanaka, *Jpn. J. Appl. Phys.*, 2021, **60**, SCCF02.

16 H. Chen, Y. Lei, X. G. Yang, C. L. Zhao and Z. Zheng, *J. Alloys Compd.*, 2021, **879**, 160348.

17 J. J. Feng, X. H. Li, Z. J. Shi, C. Zheng, X. W. Li, D. Y. Leng, Y. M. Wang, J. Liu and L. J. Zhu, *Adv. Opt. Mater.*, 2020, **8**(6), 1901762.

18 J. Song, J. Qu, M. T. Swihart and P. N. Prasad, *Nanomed. Nanotechnol.*, 2016, **12**, 771–788.

19 D. Aydemir, M. Hashemkhani, H. Y. Acar and N. N. Ulusu, *Mol. Biol. Rep.*, 2020, **47**, 4117–4129.

20 I. Tretyakov, S. Svyatodukh, A. Perepelitsa, S. Ryabchun, N. Kaurova, A. Shurakov, M. Smirnov, O. Ovchinnikov and G. Goltsman, *Nanomaterials*, 2020, **10**(5), 861.

21 M. H. Kang, S. H. Kim, S. Jang, J. E. Lim, H. Chang, K. J. Kong, S. Myung and J. K. Park, *RSC Adv.*, 2018, **8**, 28447–28452.

22 D. Chen, L. Wei, D. Wang, Y. X. Chen, Y. F. Tian, S. S. Yan, L. M. Mei and J. Jiao, *J. Alloys Compd.*, 2018, **735**, 2491–2496.

23 R. A. Ismail, A. M. E. Al-Samarai and F. M. Ahmed, *Surf. Interfaces*, 2020, **21**, 100753.

24 S. L. Tang, C. S. He, D. Li, W. H. Cai, L. Z. Fan and Y. C. Li, *J. Mater. Sci.*, 2018, **53**, 11355–11366.

25 Y. Lei, L. Y. Gu, X. G. Yang, Y. Lin and Z. Zheng, *Adv. Mater. Interfaces*, 2021, **8**(9), 2002255.

26 F. Huang, J. Z. Li, Z. H. Xu, Y. Liu, R. P. Luo, S. W. Zhang, P. B. Nie, Y. F. Lv, S. X. Zhao, W. T. Su, W. D. Li, S. C. Zhao, G. D. Wei, H. C. Kuo and F. Y. Kang, *Nanomaterials*, 2019, **9**(9), 1312.

27 Z. H. Xu, L. Tang, S. W. Zhang, J. Z. Li, B. L. Liu, S. C. Zhao, C. J. Yu and G. D. Wei, *Mater. Today Phys.*, 2020, **15**, 100273.

28 Z. G. Ji, S. C. Zhao, C. Wang and K. Liu, *Mater. Sci. Eng., B*, 2005, **117**, 63–66.

29 R. A. Ismail, D. S. Ahmed and H. A. Rawdhan, *Mater. Res. Express*, 2019, **6**(12), 125026.

30 S. I. Sadovnikov, E. G. Vovkotrub and A. A. Rempel, *Dokl. Phys. Chem.*, 2018, **480**, 2.

31 O. Alekperov, Z. Jahangirli and R. Paucar, *Phys. Status Solidi B*, 2016, **253**, 2049–2055.

32 R. W. Irene Martina, D. Jembrih-Simburger and M. Schreiner, *e-Preserv. Sci.*, 2012, **9**, 1–8.

33 C.-B. Wang, G. Deo and I. E. W. Wachs, *J. Phys. Chem. B*, 1999, **103**, 5645–5656.

34 J. J. Feng, X. H. Li, G. Q. Zhu and Q. J. Wang, *ACS Appl. Mater. Interfaces*, 2020, **12**, 43098–43105.

35 J. S. Liu, X. H. Li, Y. X. Guo, A. Qyyum, Z. J. Shi, T. C. Feng, Y. Zhang, C. X. Jiang and X. F. Liu, *Small*, 2019, **15**(38), 1970206.

36 R. Jalali, M. Parhizkar, H. Bidadi, H. Naghshara, S. R. Hosseini and M. Jafari, *Appl. Phys. A: Mater. Sci. Process.*, 2016, **122**(11), 978.

37 C. Y. Du, Y. Y. Zhao, X. J. Liu and G. Y. Shan, *J. Phys.: Condens. Matter*, 2018, **30**(42), 425502.

38 Q. Wu, M. Zhou, Y. Gong, Q. J. Li, M. Y. Yang, Q. F. Yang and Z. X. Zhang, *Catal. Sci. Technol.*, 2018, **8**, 5225–5235.

39 F. P. Yan, F. G. Yang, H. Zhang and P. H. Luo, *Mater. Res. Express*, 2021, **8**(4), 045508.

40 J. T. R. G. A. Vancu, *Phys. Status Solidi B*, 1966, **15**, 627–637.

41 J. V. M. Lima, S. B. O. Santos, R. A. Silva, M. H. Boratto, C. F. O. Graeff and L. V. A. Scalvi, *J. Mater. Sci.: Mater. Electron.*, 2021, **32**, 21804–21812.

42 S. H. Kim, J. Lim, S. Lee, M. H. Kang, W. Song, J. Lim, S. Lee, E. K. Kim, J. K. Park and S. Myung, *RSC Adv.*, 2021, **11**, 22625–22632.

43 X. Peng, Y. F. Lv, L. Fu, F. Chen, W. T. Su, J. Z. Li, Q. Zhang and S. C. Zhao, *RSC Adv.*, 2021, **11**, 34095–34100.

44 M. Law, H. Kind, B. Messer, F. Kim and P. Yang, *Angew. Chem., Int. Ed.*, 2002, **41**, 2405–2408.